



Removal of DPM from an Air Stream Using Micron-Scale Droplets

Lucas Rojas-Mendoza¹, Emily A. Sarver^{1*}, John R. Saylor²

¹ *Department of Mining and Minerals, Virginia Tech, Blacksburg, VA 24060, USA*

² *Department of Mechanical Engineering, Clemson University, Clemson, SC 29634, USA*

ABSTRACT

Respiratory exposures to diesel particulate matter (DPM) present health risks, particularly in confined environments with a relatively high number of emission sources. Despite a variety of existing control technologies, exposures in some occupational environments remain unacceptably high (e.g., underground mine environments), and new technologies and abatement strategies are needed. The physics of droplet-particle interactions suggests that micron-scale water drops can effectively scavenge DPM from an air stream. Here, experimental results are presented on DPM removal from a diesel exhaust stream using a fog of water droplets. Measured scavenging coefficients, based on both number density and mass, show that significant DPM removal is possible. The potential scavenging mechanisms at play are discussed, and insights are offered on future work necessary for scale-up of a fog-based exhaust treatment technology.

Keywords: Diesel particulate matter (DPM); DPM removal; DPM coagulation; Micron-scale water drops.

INTRODUCTION

Diesel-powered engines are extensively used in industrial activities (United States Department of Labor, 2013). Diesel exhaust contains a mixture of gases and very small particles (Kittelson, 1997; Bugarski *et al.*, 2011). The solid fraction of the exhaust is called diesel particulate matter (DPM), and consists mainly of elemental carbon, organic carbon and sulfur compounds (Kittelson, 1997; Jin *et al.*, 2017).

In terms of size, DPM particles are typically classified into two modes: the nuclei mode which is composed of volatile particulates in the nanoparticle range (< 50 nm); and the accumulation mode which includes larger particulate (50–1000 nm) made of carbonaceous material with adsorbed hydrocarbons and sulfates (Kittelson, 1997). In terms of number, the majority of the particles reside in the nuclei mode, while most of the mass resides in the accumulation mode (Kittelson, 1997; Bugarski *et al.*, 2011).

DPM is recognized as an environmental and occupational hazard (Bugarski *et al.*, 2009). Due to its size, it can penetrate deep into the respiratory system, and inhalation can lead to chronic cardiovascular and respiratory diseases (U.S. Department of Labor, 2013). DPM is now classified as a human carcinogen, and epidemiological studies have indicated that occupational exposures can result in increased

risk of lung cancer (Ravindra *et al.*, 2008; NTP, 2016). While toxicological mechanisms are not fully understood, the ultrafine nature of DPM is likely a key factor in the dose-response effect. Indeed, numerous studies have concluded that deleterious health effects of many nanoscale particles scale to their size and number density rather than mass (Dockery *et al.*, 1993; Pope *et al.*, 1995; Tetley, 2007; Kumar *et al.*, 2010), and some toxicological studies show that even normally inert compounds such as gold (Coradeghini *et al.*, 2013; Hongxia, 2016), copper oxide (Karlsson *et al.*, 2009) and Teflon (Warheit *et al.*, 1990) can cause cell damage when exposures occur in the form of nanoparticles versus larger particles.

To curb DPM exposures, a number of controls have been developed. These include low emission engines, cleaner fuels, and exhaust treatments such as diesel particulate filters and oxidation catalysts (Bugarski *et al.*, 2009; Bugarski *et al.*, 2010; Hsieh *et al.*, 2011; Tsai *et al.*, 2015). However, DPM exposures remain relatively high in some environments (e.g., underground mines, truck loading depots) (Bugarski *et al.*, 2010, 2011) – either because adoption of controls is not feasible or not sufficient. Underground miners generally experience the highest exposures (versus other occupations) due to use of equipment in confined spaces (Grau *et al.*, 2002). Even with controls in place, adequate reduction of DPM levels in some mines is a challenge because the necessary ventilation is not practicable (Grau *et al.*, 2004, 2006; Noll *et al.*, 2008).

While particle size is increasingly recognized as a major factor in exposure-response relationships for respirable particles (Gomes *et al.*, 2013a, b), occupational DPM exposures are generally measured based on mass

* Corresponding author.

Tel.: +1 540 231 8139; Fax: 1-540-231-4070

E-mail address: esarver@vt.edu

concentrations (*Code of Federal Regulations Title 30 Part 57 Section 5066 (30CFR57.5066)*) which are less sensitive to smaller particles. Consequently, the effectiveness of DPM controls has been most often assessed in terms of mass removal (Bugarski *et al.*, 2009). In light of the above, it is critical to explore and apply new technologies in order to reduce both mass-based and number-based exposures.

Water sprays are ubiquitous in industry as part of respirable particle exposure controls (Kim *et al.*, 2001; Copeland, 2007; Pollock and Organiscak, 2007). They are mainly used in wet scrubbers and by direct application in very dusty areas (Kim *et al.*, 2001; Copeland, 2007; Ha *et al.*, 2009). Water sprays are effective in reducing particle loading in the air through two major mechanisms: wetting suppression, in which water drops are applied to surfaces to prevent particles from becoming airborne; and particle scavenging, in which suspended particles are brought into contact with water droplets which are then removed via gravitational settling (Kim *et al.*, 2001; NTP, 2010). The effectiveness of particle scavenging by water drops is highly dependent on the particle and drop diameters, densities, number concentrations, air properties, and other factors (Kim *et al.*, 2001; Ran *et al.*, 2014; Di Natale *et al.*, 2015; Di Natale *et al.*, 2016). Particle diameters play a particularly large role in determining the efficiency of particle removal by drops (Ran *et al.*, 2014). Particle removal by drops is dominated by particle inertia at diameters larger than a micron (Hinds, 1999) while inertia is essentially negligible for nanometer-scale particles (Kim *et al.*, 2001), and where diffusive effects due to Brownian motion of particles becomes the dominant scavenging mechanism (Hinds, 1999; Tran *et al.*, 2009; Ran *et al.*, 2014).

While fundamental fluid mechanics and preliminary

studies suggest that drop scavenging can affect both large and small particles via different mechanisms (i.e., inertia and diffusion), only a few experimental studies have been identified that directly relate to the applicability of spray treatments on the removal and control of DPM or other combustion-related particulates. These studies used drops that were larger than 100 μm in diameter and showed that particle and/or drop charging was often necessary to achieve significant removal (Tran *et al.*, 2009; Di Natale *et al.*, 2015). In contrast to the approach of forcing water drops and DPM particles to combine, Tsai *et al.* (2005) used a fine water mist to cool a submicron particle-laden flow, which was then passed through a Venturi scrubber. Between the cooling and pressure drop induced by the scrubber, sufficient condensation occurred on the particles to increase their size to the point where the scrubber could effectively remove them.

The objective of the work presented here was to investigate the efficacy of using micron-scale water droplets to remove DPM from a diesel exhaust stream in a laboratory environment. Results are presented to show how application of a fog of water droplets improved DPM removal in terms of both number density and mass.

METHODS

A schematic of the experimental apparatus is shown in Fig. 1. The overall approach of the experiments was to direct a flow of diesel exhaust through a chamber where a fog of water drops is introduced, and to measure the DPM upstream and downstream of the chamber. The percent DPM removal based on number density or mass was then obtained as

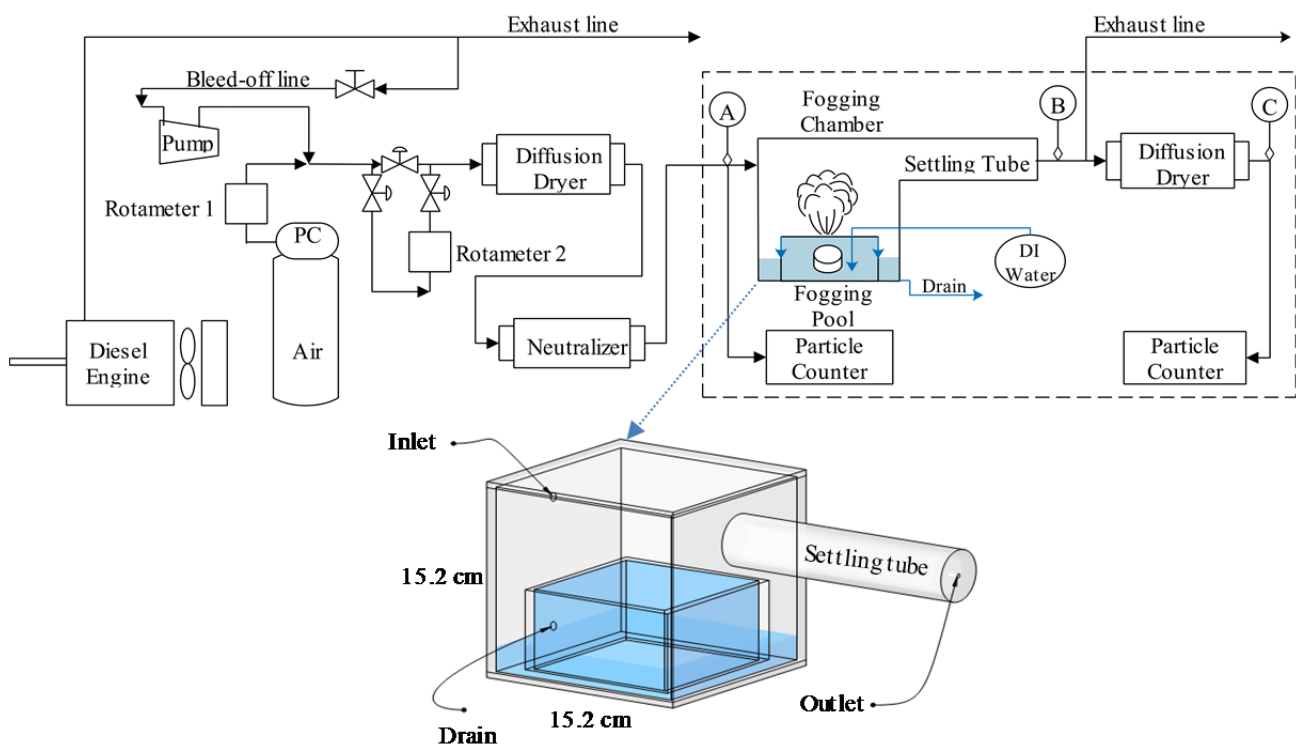


Fig. 1. DPM scavenging experimental apparatus. Locations A, B, and C are sampling locations.

$$L_N (\%) = \left(\frac{C_U - C_D}{C_U} \right) \times 100 \quad (1)$$

or

$$L_M (\%) = \left(\frac{M_U - M_D}{M_U} \right) \times 100 \quad (2)$$

respectively, where C_U and C_D are the upstream and downstream particle number densities ($\# \text{ cc}^{-1}$), and M_U and M_D are the mass of DPM samples collected upstream and downstream, respectively.

A Kubota EA330-E4-NB1 engine (Lincolnshire, IL) served as the DPM source. The engine was run on idle for all experiments, and had a speed of approximately 2200 RPM under this condition. A fractional bleed-off of the diesel exhaust was drawn via a small diaphragm pump. For experiments to measure number density, the raw exhaust was conditioned by 1) dilution with clean air, which was necessary to reduce the DPM number concentration to within the measuring range of the particle counters; 2) passing the flow through a diffusion dryer to ensure that drops were not counted as DPM; and 3) neutralization of surface charges using a TSI Kr-85 neutralizer (Shoreview, MN). High-resolution flow meters were used to measure flow rates.

After conditioning, the DPM-laden air was directed into the treatment stage (dashed area in Fig. 1). The fogging chamber (Fig. 1) is an acrylic box composed of two reservoirs: a sealed outer cube and an inner water pool. From the surface of the pool, fog droplets were generated within the chamber, as described below. Deionized (DI) water was fed to the pool at a rate of 0.9 L min^{-1} , causing it to overflow onto the chamber floor where it drained slowly from the system. This design ensured that any diesel components that contaminated the water surface were quickly removed from the system. Detailed drawings of the fogging chamber can be seen in Fig. S1 in the supplementary files.

The fog-generating device or “fogger” used here was a 24 W submersible ultrasonic transducer. Acoustic energy from the transducer is directed upward through the water to the air-water interface, resulting in the formation of water droplets with a mean diameter of approximately $3.9 \mu\text{m}$ (with 95% of water drops falling within $1.9\text{--}7.3 \mu\text{m}$) and a number density of about $5.0 \times 10^5 \text{ drops cc}^{-1}$ (for the flow rates investigated here). The size of the water droplets was determined by allowing the drops to impact a glass slide, and then by imaging them with a Zeiss Axiovert 200M MAT stereoscope microscope (Oberkochen, Germany)

coupled with a digital camera (AxioCam MRc 5). Images were processed using ImageJ (NIH, Bethesda, MA).

The combination of DPM and fog flowed from the chamber into an acrylic settling tube (inner diameter of 4.45 cm) with a length of either 61 cm or 183 cm, referred to hereinafter as the “short” and “long” tube, respectively. Use of these two tubes enabled different durations of DPM-fog interaction, at a given flow rate. DPM number densities were measured at locations A and C (Fig. 1) using a pair of identical particle counters (NanoScan SMPS Nanoparticle sizer 3910, TSI, Shoreview, MN). The NanoScan instrument is a spectrometer that counts and sizes particles from 10–420 nm, which are classified into 13 size bins, and makes measurements at a frequency of 1 measurement/min. Mass samples were acquired at locations A, B, and C by using a pump to aspirate a fraction of the air stream through a non-hydroscopic polycarbonate (PC) filter.

Experiments to Determine DPM Removal Based on Number Density (L_N)

Measurements of DPM number density were obtained at locations A and C; L_N (Eq. (1)) was computed using A as the upstream location and C as the downstream location. (Number density measurements could not be made at location B since the particle counters require a dry airflow.) L_N values correspond to DPM losses across the entire system, including removal occurring in the fogging chamber/settling tube and in the diffusion dryer. Four test conditions were considered: fogger on versus fogger off, each using the short and the long settling tube. These four conditions are listed in Table 1. Data was collected during four different engine runs, two using the short tube and two using the long tube. In each engine run, both fog treatments (i.e., on and off) were randomly assigned and tested twice. Each fogging condition test consisted of 5 one-minute measurements (i.e., 20 measurements in each engine run). A 5-minute lag was introduced in between tests to ensure that any possible carryover effect from the previous condition was not considered. Values for L_N were calculated for each of the 13 particle size bins provided by the NanoScan. In total, 80 pairs of measurements were obtained at locations A and C.

The engine was warmed-up for 60 minutes to ensure a steady-state exhaust condition before data was collected. During this period, and for 10 minutes at the end of each experiment, the NanoScans were run in parallel at location A to confirm correlation between their measurements. When evaluating NanoScan data for the sum of all 13 particle size bins, no correction was necessary as the two instruments differed on average by only 0.6%, and the correlation coefficient between the two instruments was greater than

Table 1. Conditions for DPM removal based on number densities.

Engine Run/ Tube Length	Fog treatment test sequence				Engine RPM
	1 st	2 nd	3 rd	4 th	
1-long	ON	OFF	OFF	ON	2193
2-short	ON	OFF	ON	OFF	2199
3-short	OFF	ON	ON	OFF	2187
4-long	ON	OFF	ON	OFF	2193

0.99 during these check runs. When looking at individual size bins, paired number density-measurements were used to build calibration curves between NanoScan1 and NanoScan2 (i.e., for each individual size bin). Results are presented here only for the five size bins that could be linearly related to one another. The diameter ranges corresponding to these five bins were: 23.7–31.6 nm; 31.6–42.2 nm; 42.2–56.2 nm; 56.2–75 nm; 75–100 nm. For all of these bins, the linear calibration curve between NanoScan 1 and NanoScan 2 had correlation coefficients greater than 0.90. Moreover, these five bins were consistently observed to account for more than 92% of the total number of DPM particles at location A.

After warming up and collecting paired measurements at location A, one NanoScan unit was moved to location C. Then, as an additional check, 8.5 L min⁻¹ of dilution air (and no DPM) was introduced into the fogging chamber while the fogger was on in order to determine background particulate concentration due to the water itself. Such particles exist due to the finite amount of contaminants in DI water, which remain as particles when the droplets evaporate. Upon successful completion of these checks, data was acquired following the sequence shown in Table 1. This background particulate concentration was $< 4.0 \times 10^4$ particles cc⁻¹.

For the entire course of these experiments (i.e., 80 1-minute samples) the average DPM number density at location A was $1.36 \times 10^6 \pm 0.03 \times 10^6$ particles cc⁻¹ (i.e., 95% confidence interval for the average value). The background concentration of particles associated with fog droplets was $< 4.0 \times 10^4$ particles cc⁻¹, as noted above, and this level represented less than 3% of the mean DPM number density at location A. The background concentration of particles in the dilution air was negligible (< 1.0 particle cc⁻¹). The dilution ratio was kept constant for all experiments at 5.0 L min⁻¹ of diesel exhaust to 3.5 L min⁻¹ of dilution air.

The average engine speed was 2193 RPM and varied by $< 1\%$ for all experiments, as shown in Table 1. The particle counter sampling in location A, NanoScan1, operated at a sampling rate of 0.745 L min⁻¹ and the particle counter in location C, NanoScan2, operated at a sampling rate of 0.800 L min⁻¹. The total flow through the fogging chamber was estimated at 7.8 L min⁻¹, which is the total diluted DPM-laden airflow minus the NanoScan1 sampling rate.

Experiments to Determine DPM Removal Based on Mass (L_M)

As mentioned above, DPM number density could not be measured at location B, so L_N values can only be used to determine the removal of DPM particles across the entire system. To determine the removal coefficients for the chamber/tube and for the diffusion dryer separately, mass-based experiments were also performed. For these, DPM mass samples were collected at locations A, B, and C, such that L_M (Eq. (2)) could be obtained between locations A and B and locations A and C. The mass loss between A and B is attributed to DPM removal in the chamber/tube; and the difference between losses from A to B and A to C is attributed to removal in the downstream diffusion dryer. These experiments used the long settling tube, and the fog-on and fog-off treatment conditions were run sequentially,

each for 150 minutes (i.e., during a single engine run for each experiment).

Samples were collected on PC filters with a measured retention efficiency of approximately 97% across the entire size range of the NanoScan. The flow rate of the sampling pumps was set to 1.7 L min⁻¹. Any moisture in the samples was removed by drying the PC filters in a 40 deg C oven after they were removed from the experimental apparatus. The filters were weighed before and after sample collection using a Sartorius Cubis MSE6.6S microbalance (Göttingen, Germany). The dilution ratio was fixed at 5.5 L min⁻¹ of diesel exhaust to 4 L min⁻¹ of ultra-zero dry air during these runs, and the total flow through the fogging chamber was estimated at 7.8 L min⁻¹ as was the case for the number density experiments. The engine speed was 2200 RPM and the engine was again warmed-up for 60 minutes' prior sample collection.

Analysis of number- and mass-based data were conducted with the JMP pro 11 statistical package (SAS, Cary, NC).

RESULTS AND DISCUSSION

DPM removal Based on Number Density (L_N)

Fig. 2 shows time traces of DPM number densities at locations A and C for the fog-off and fog-on conditions for each engine run. When the fogger was turned off, the system was considered to be in "deposition mode," meaning that the DPM which is lost in this mode is due simply to deposition on surfaces. When the fogger was on, the system was considered to be in "scavenging mode," meaning particles are removed through both drop removal and deposition.

As the plots show, the presence of fog reduces the number concentration at location C for nominally constant concentrations at location A. As mentioned above, the average DPM concentration at location A was consistent across all tests, with an average value of $1.36 \times 10^6 \pm 0.03 \times 10^6$ particles cc⁻¹. When the fog was off, the average concentration at location C was $7.71 \times 10^5 \pm 0.44 \times 10^5$ particles cc⁻¹; and when the fog was on, the average concentration was $1.66 \times 10^5 \pm 0.13 \times 10^5$ particles cc⁻¹. These measurements were used to obtain values for L_N via Eq. (1). An average L_N value was calculated for each fog treatment condition (see Table S1 in supplementary files) over the entire size range investigated (i.e., 10–420 nm). Values of L_N for all fog-off and all fog-on conditions were averaged across tests for each tube length, and the improvement in DPM removal attributed to the fog was calculated (i.e., average removal during the fog-on condition minus average removal during the fog-off condition). These results are presented in Fig. 3 and clearly show that in every case significantly more DPM is removed with the fogging treatment. There was no statistically significant effect of the tube length, however. The reason for this will be discussed below. The average improvement in L_N due to fog across both tube lengths was $45.1\% \pm 7.0\%$.

DPM Removal Based on Number Density (L_N) for Different Size Ranges

Using the same analysis as above for the total particle

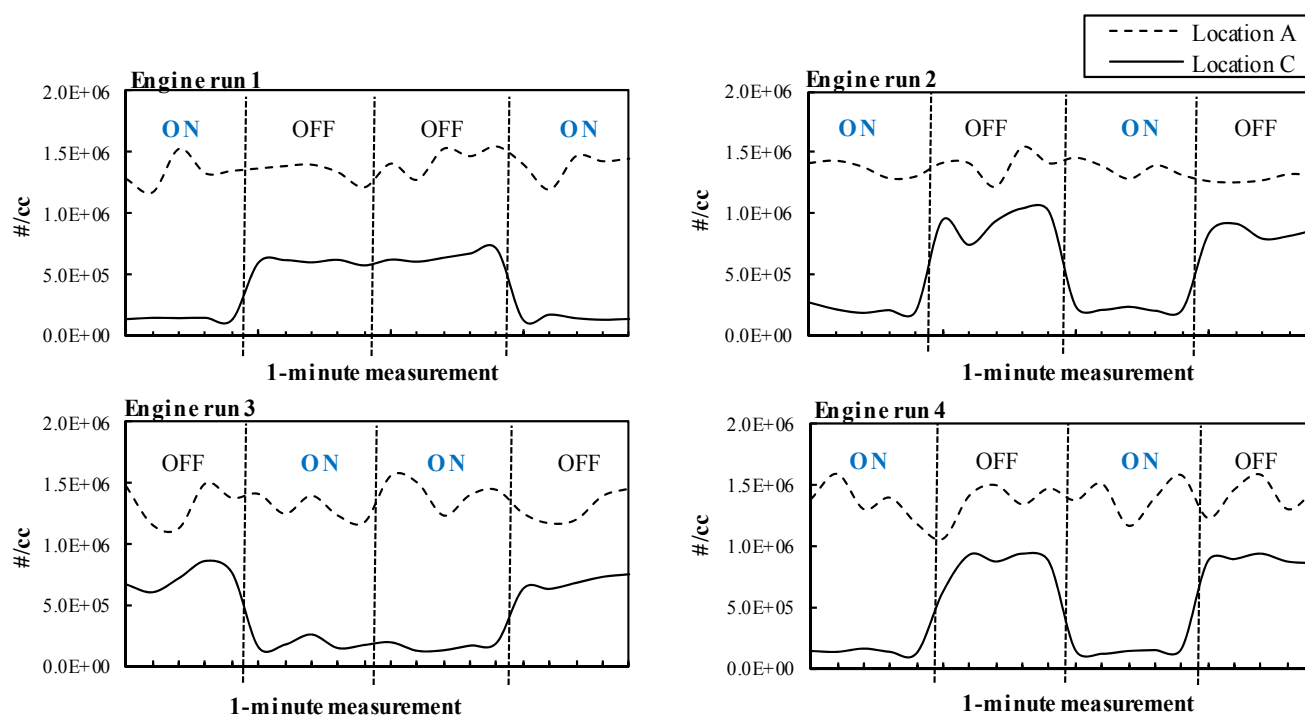


Fig. 2. Time traces of number-based DPM concentration at locations A and C. Number concentrations represent the total of all particle diameters between 10–420 nm. The much wider difference between A-C with fog-on vs. fog-off indicates significant improvement in DPM removal with the fog treatment.

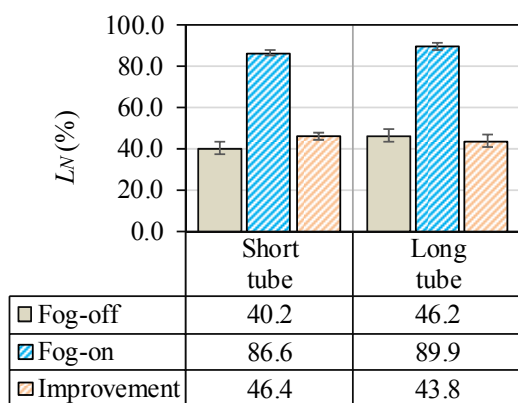


Fig. 3. Average L_N values (between locations A and C) for each treatment condition accounting for all particles between 10–420 nm. Error bars represent 95% confidence intervals.

counts, a value for L_N was computed for each of the five individual size bins that are considered here: 23.7–31.6 nm; 31.6–42.2 nm; 42.2–56.2 nm; 56.2–75 nm; 75–100 nm. As shown in Fig. 4, the fog treatment significantly increases DPM removal in all five bins. It is also clear from the figure that the improvement in removal is fairly similar across these bins. Average improvements in particle removal due to the application of the fog treatment ranged from 39.6% to 54.6%.

DPM Removal Based on Mass (L_M)

Mass samples were obtained from locations A, B, and C. For each set of measurements, L_M was computed using Eq. (2)

between A and B, and also between A and C (Fig. 5); the difference between these values is attributed to DPM removal in the downstream diffusion dryer. Results showed that the fog treatment improved DPM mass removal across the entire system (A-C) by an average of 15.5%, and in the chamber/settling tube (A-B) by an average of 20.2%. The effect of the diffusion dryer was observed to be relatively small. It was responsible for removing 7.0% of the DPM mass in the fog-off condition (versus a total mass removal of 45.4% across the entire system), and just 2.4% in the fog-on condition (versus 60.9% across the entire system). Photographs of samples for each treatment condition can be seen in Fig. 6. This provides visual evidence that, on a mass basis, more DPM is being removed from the system during the fog-on condition.

Analysis

The experimental data suggests that the fog treatment resulted in significant improvement in DPM removal. In terms of number density, removal between locations A and C was improved by about 45% with no significant variation across the five size bins studied. In terms of mass, the improvement in removal was estimated at 15.5%, with minimal removal occurring at the diffusion dryer.

Assuming that the increase in removal is due to contact between DPM particles and water drops, then the increases in L_N and L_M due to the presence of fog must be due to the subsequent removal of particle-containing drops. Possible mechanisms for removal of such drops include gravitational settling; impact of the drops with the internal walls of the system due to inertial effects when the flow changes

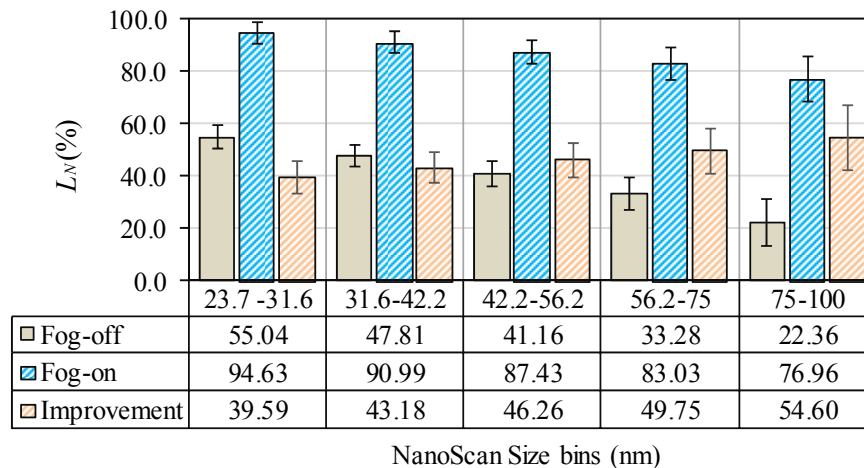


Fig. 4. Values of L_N for each of the five size bins for the fog-on and fog-off conditions, as well as the percent improvement due to fog. Error bars represent 95% confidence intervals.

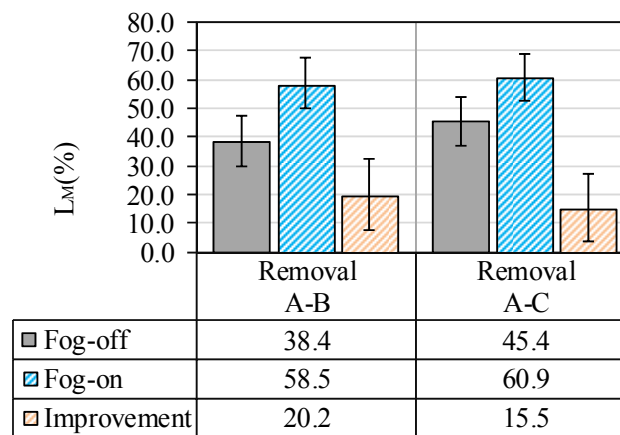


Fig. 5. Mass-based DPM removal (L_M) between locations A and B and locations A and C. Error bars represent 95% confidence intervals.

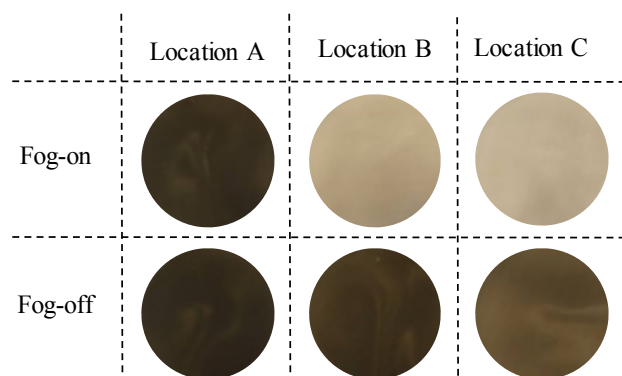


Fig. 6. Photographs of filters collected during mass-based experiments at locations A, B and C.

direction and/or due to turbulence in the flow; and impact with the drying media in the diffusion dryer. Each of these is explored in turn to ascertain their possible contribution to the observed results.

First, however, the means by which the particles come into contact with the drops must be addressed. This combination, or coagulation, of particles with drops can occur through a

variety of mechanisms, but for the conditions explored in these experiments it is likely to be due to two main mechanisms: kinematic coagulation and thermal coagulation (Hinds, 1999). Kinematic coagulation occurs as a result of relative motion between particles and can occur due to differential settling between water droplets and DPM, and/or as a result of turbulence in the system. Turbulence is

not expected to be a significant factor here as the Reynolds numbers for the chamber and the settling tube were estimated to be about 10 and 1000, respectively. The rate of collisions between small and large particles due to differential settling is described by (Hinds, 1999):

$$\frac{dN}{dT} = \frac{\pi}{4} d_d^2 V_{TS} NE \quad (3)$$

where, d_d is the diameter of the water drop, V_{TS} is the relative velocity between drops and particles at their terminal settling velocity, N is the number density of particles, and E is the collisional efficiency. E is a function of the Stokes number, Stk , defined as:

$$Stk = \frac{\rho_p d_p^2 C_c V_{TS}}{18\eta d_d} \quad (4)$$

where ρ_p is the particle density, d_p is the particle diameter, C_c is the slip correction factor and η is the air viscosity. According to Eq. (3), significant particle collection will occur for large collisional efficiency. However, the efficiency is low except for the scenario where particles and drops are a few micrometers or larger (Hinds, 1999). Therefore, the effect of kinematic coagulation (due to impaction) should be negligible for the present system with nanometer-scale DPM particles.

Thermal coagulation, on the other hand, is driven by Brownian motion of particles. Its effect is significant for very small particles, and increases further in systems containing a combination of large and small particles (Hinds, 1999) – such is the case here, where nanometer-scale DPM particles interact with micron-scale water droplets. For this system, the rate of change in number density due to thermal coagulation can be described by (Hinds, 1999):

$$\frac{dN}{dt} = -KN^2 \quad (5)$$

where N is the total number density of the aerosol (i.e., DPM number density plus water drops number density) and K is the coagulation coefficient which depends on the size of all particles involved; its calculation is complicated for poly-dispersed aerosols.

Assuming monodisperse distributions of DPM (i.e., with a diameter of 46 nm, which was the geometric mean diameter of all exhaust particles counted by the Nanoscan at location A) and water drops (i.e., with diameter of 3.9 μm), Eq. (5) can be integrated for the conditions of these experiments. The mean DPM concentration across all Nanoscan size bins was 1.36×10^6 particles cc^{-1} ; and that of the water droplets was approximately 5.0×10^5 drops cc^{-1} . Due to the relative size difference between water droplets and DPM particles, the coagulation coefficient can be calculated as:

$$K_{d-p} \cong \pi(d_d D_p) \quad (6)$$

where d_d is the diameter of the water drops and D_p is the diffusivity coefficient for DPM particles:

$$D_p = \frac{kTC_c}{3\pi\eta d_p} \quad (7)$$

where d_p is the diameter of DPM, k is the Boltzmann's constant and T is the absolute temperature. Based on the above, coagulation between water droplets and DPM particles should proceed approximately 100 times faster than coagulation of DPM particles with each other, or water drops with each other. Therefore, only the interactions between DPM and water drops will be considered. Integrating Eq. (5), the total concentration of DPM and water drops as a function of time is:

$$N(t) = \frac{N_o}{1 + KN_o \times t} \quad (8)$$

where N_o is the total initial concentration obtained by summing DPM and water drop number densities, and K is the coagulation coefficient between drops and DPM particles. Finally, the total DPM number density as a function of time, $N_p(t)$ was calculated by:

$$N_p(t) = \frac{N_o}{1 + KN_o \times t} - N_d \quad (9)$$

where N_d is the number density of water drops, which is assumed to be constant.

For this analysis, it is assumed that once a DPM particle comes together with a water drop, the particle remains attached. Additionally, any change in concentration is due to the effective disappearance of DPM particles and not water droplets, which should essentially preserve their original size upon coagulation with a DPM particle.

The percent of DPM attaching to water droplets as a function of time can then be estimated by comparing the present DPM number density (i.e., airborne DPM in the system which is not attached to water drops) to the original number density. Fig. 7 shows the fraction of attachment expected during the maximum residence time considered here (i.e., 65 seconds with the long settling tube). The residence time for the fogging chamber alone was calculated to be about 43 s (i.e., dividing the total volume of the chamber and settling tube by the volumetric flow rate through them). Similarly, the residence time for each tube length was calculated to be 7 and 21 s for the short and long tube, respectively.

Under the given conditions and assumptions, the fraction of particles attached to water droplets reached an asymptotic value (i.e. near the unity) at about 40 s. This means that no significant extra attachment would be expected for increased residence time beyond this point, and therefore most of the attachment occurs in the fogging chamber. This analysis is in general agreement with the experimental results, which showed no change in L_N with increasing tube length.

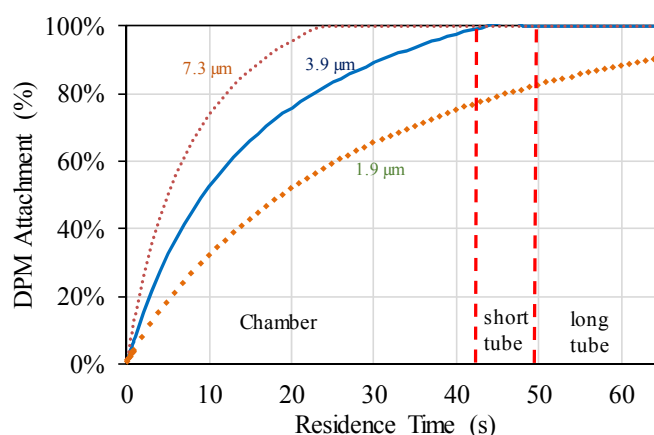


Fig. 7. DPM attachment as a function of residence time.

Although the analysis assumes that all water drops have a diameter of 3.9 μm , as noted above 95% of the drops fell within 1.9 μm and 7.3 μm in diameter. To check the effect of this variation, Fig. 7 shows also the fraction of attachment expected during the maximum residence time if all water drops were 1.9 or 7.3 μm in diameter (see dashed lines above and below solid line in the figure). Thus, larger droplets are not expected to significantly change the DPM-drop attachment at the given residence times - though they would be subject to much faster gravitational settling. Smaller drops, on the other hand, would be subject to slower settling and would yield an expected attachment of 77% at the exit of the chamber, increasing to 82% at the exit of the short settling tube.

Having demonstrated that thermal coagulation can result in significant DPM-droplet combinations, an explanation for how these particle-drop combinations may be eliminated from the system is needed. As noted above, this could be due to gravitational settling, inertial effects, or impact with the media in the diffusion dryer. Given the relatively small Reynolds numbers in the system, it is unlikely that inertial effects due to rapidly changing turbulent flow paths result in inertial removal of particle-laden drops. Furthermore, the changes in direction of the flow due to the geometry of the system are expected to be small and localized, also suggesting that inertial effects do not explain removal of particle-laden drops - at least in portions of the system outside of the diffusion dryer.

To assess the possibility that drop removal between locations A and B is governed by settling, the drop settling time can easily be compared with the system residence time. For 3.9 μm drops, the settling velocity is $1.44 \times 10^{-3} \text{ m s}^{-1}$, obtained using the equation for terminal velocity of a spherical drop:

$$V_T = \frac{g\rho_d d_d^2}{18\eta} \quad (10)$$

where g is the gravity constant and ρ_d is the density of the water drop. Using the aforementioned residence time for the chamber only, the drop number density should be

reduced due to gravitational settling by 26% at the exit of the chamber. If the short tube is used, the total reduction should be about 38% at the exit of tube; and if the long tube is used, the total reduction should be about 42%. Assuming that DPM-drop attachment is homogenous (i.e., the DPM is homogeneously distributed among the drops) then the settling of each water drop should be associated with an incremental decrease in DPM number density (and increase in DPM removal).

Taking the predicted settling of water drops together with the coagulation analysis, which indicates near 100% attachment by the time the drops reach the end of the fogging chamber (Fig. 7), a total DPM number removal due to the fog treatment is estimated at 42% between locations A and B. If the diffusion dryer does not in fact significantly remove particles (as the mass-based results suggest), then the estimated DPM number removal expected due to coagulation and settling is consistent with the experimental results (i.e., about 42 vs. 45%).

The mass-based results reported here can be considered as further support for the proposed two-step mechanism. While number-based measurements were not possible at location B, the mass-based measurements showed that the fog removed about 20% of the DPM between A and B (see Fig. 5). This value is in reasonable agreement with the 45% DPM number removal, especially considering that the mass and number results should not be regarded as directly comparable. Indeed, the mass measurements probably included particles that the number-based measurements did not (i.e., diameters greater than about 400 nm). Consider, for example, the likely case where a relatively small number fraction of the DPM particles are relatively large in size (e.g., nearing 1 μm). In this case, the water drops may not significantly interact with the larger particles (i.e., due to slower coagulation rates between DPM and drops as the two near each other in size), effectively resulting in relatively low DPM mass removal but relatively high number removal.

CONCLUSIONS

The work presented here demonstrates that micron-scale water drops (fog), may be employed to remove nano-scale

DPM from an exhaust stream. Though further work is required to confirm the exact mechanism of DPM removal, DPM-water droplet attachment followed by droplet removal provides a likely explanation. Given the limited scope of results presented in this study, an investigation of additional conditions is necessary to demonstrate the applicability of such a treatment for real diesel exhaust streams. Future research should focus on raw exhaust and the effect of the treatment under shorter residence times, or higher exhaust velocities, as this would better represent practical conditions. Other factors to consider in a scaled-up treatment scheme include temperature, engine loading, pressure drop, and water consumption.

ACKNOWLEDGMENTS

The authors would like to thank the CDC/NIOSH office of Mine Safety and Health Research (OMSHR) for funding this work (contract no. 200-2014-59646). Findings and conclusions expressed here are those of the authors and do not necessarily represent those of the funding source.

SUPPLEMENTARY MATERIAL

Supplementary data associated with this article can be found in the online version at <http://www.aaqr.org>.

REFERENCES

- Bugarski, A.D., Schanakenberg, G.H., Hummer, J.A., Cauda, E., Janisko, S.J. and Patts, L.D. (2009). Effects of diesel exhaust aftertreatment devices on concentrations and size distribution of aerosols in underground mine air. *Environ. Sci. Technol.* 43: 6737–6743.
- Bugarski, A.D., Cauda, E., Janisko, S.J., Hummer, J.A. and Patts, L.D. (2010). Aerosols emitted in underground mine air by diesel engine fueled with biodiesel. *J. Air Waste Manage. Assoc.* 60: 237–244.
- Bugarski, A.D., Janisko, S.J., Cauda, E.G., Noll, J.D. and Mischler, S.E. (2011). *Diesel Aerosols and Gases in Underground Mines: Guide to Exposure Assessment and Control*, Department of Health and Human Services, Public Health Service, Centers for Disease Control and Prevention, National Institute for Occupational Safety and Health, DHHS (NIOSH) Publication No. 2012-101 (RI 9687), Pittsburgh, PA, USA, <http://www.cdc.gov/niosh/mining/UserFiles/works/pdfs/2012-101.pdf>.
- Code of Federal Regulations Title 30 Part 57 Section 5066 (30CFR57.5066); Limit on Exposure to Diesel Particulate Matter, 2013.
- Colinet, J.F., Rider, J.P., Listak, J.M., Organiscak, J.A. and Wolfe, A.L. (2010). *Best Practices for Dust Control in Coal Mining*. Department of Health and Human Services, Public Health Service, Centers for Disease Control and Prevention, National Institute for Occupational Safety and Health, DHHS (NIOSH) Publication No. 2010-110 (IC 9517), Pittsburgh, PA, USA. <http://www.cdc.gov/niosh/mining/UserFiles/works/pdfs/2010-132.pdf>.
- Copeland, C.R. (2007). *Suppression and Dispersion of Airborne Dust and Nanoparticulates*. Ph.D. Dissertation, Michigan Technological University, Houghton, MI.
- Coradeghini, R., Gioria, S., Garcia, C.P., Nativo, P., Franchini, F., Gilliland, D., Ponti, J. and Rossi, F. (2013). Size-dependent toxicity and cell interaction mechanisms of gold nanoparticles on mouse fibroblasts. *Toxicol. Lett.* 217: 205–216.
- Di Natale, F., Carotenuto, C., D'Addio, L., Jaworek, A., Krupa, A., Szudyga, M. and Lancia, A. (2015). Capture of fine and ultrafine particles in a wet electrostatic scrubber. *J. Environ. Chem. Eng.* 3: 349–356.
- Di Natale, F., Carotenuto, C., D'Addio, L. and Lancia, A. (2016). Effect of gas temperature on the capture of charged particles by oppositely charged water droplets. *Aerosol Sci. Technol.* 50: 110–117.
- Dockery, D.W., Pope, A., Xu, X., Spengler, J.D., Ware, J.H., Fay, M.E., Ferris, B.G. and Speizer, F.E. (1996). An Association between Air Pollution and Mortality in Six U.S. cities. *J. Med.* 329: 1753–1759.
- Gomes, J.F., Albuquerque, P.C., Esteves, H.M. and Carvalho, P.A. (2013a). Notice on a methodology for characterizing emissions of ultrafine particles/nanoparticles in microenvironments. *Energy Emissions Control Technol.* 1: 15–27.
- Gomes, J.F., Guerreiro, C., Lavrador, D., Carvalho, P.A. and Miranda, R.M. (2013b). TEM analysis as a tool for toxicological assessment of occupational exposure to airborne nanoparticles from welding. *Microsc. Microanal.* 19: 153–154.
- Grau, R.H., Mucho, T.P., Robertson, A.C., Smith, A.C. and Garcia, F. (2002). Practical techniques to improve the air quality in underground stone mines, Proc. 9th North Am. U.S. Mine Vent. Symp, 2002, pp. 123–129. <https://www.cdc.gov/niosh/mining/UserFiles/works/pdfs/ptoit.pdf>.
- Grau, R.H., Robertson, S.B., Krog, R.B., Chekan, G.J. and Mucho, T.P. (2004). Raising the bar of ventilation for large-opening stone mines, Proc. 10th North Am. U.S. Mine Vent. Symp, 2004, pp. 349–355, <http://www.cdc.gov/niosh/mining/works/coverSheet445.html>.
- Grau, R.H., Krog, R.B. and Robertson, S.B. (2006). Maximizing the ventilation of large-opening mines, Proc. 11th North Am. U.S. Mine Vent. Symp, 2006, pp. 53–60, <http://www.cdc.gov/niosh/mining/pubs/pubreference/outputid1979.htm>.18.
- Ha, T.H., Nishida, O., Fujita, H. and Wataru, H. (2009). Simultaneous removal of NO_x and fine diesel particulate matter (DPM) by electrostatic water spraying scrubber. *J. Mar. Eng. Technol.* 8: 45–53.
- Hinds, W.C. (1999). *Aerosol Technology. Properties, Behavior and Measurement of Airborne Particles*, 2nd ed., Wiley-Interscience, New York.
- Hongxia, L. (2016). Size-dependent genotoxicity of gold nanoparticles in the comet assay and long-term in vivo micronucleus test. *Toxicol. Lett.* 258: S54.
- Hsieh, L.T., Wu, E.M., Wang, L.C., Chang-Chien, G.P. and Yeh, Y.F. (2011). Reduction of toxic pollutants emitted from heavy-duty diesel vehicles by deploying diesel

- particulate filters. *Aerosol Air Qual. Res.* 11: 709–715.
- Jin, T., Lu, K., Liu, S., Zhao, S., Qu, L. and Xu, X. (2017). Chemical characteristics of particulate matter emission from a heavy-duty diesel engine using ETC cycle dynamometer test. *Aerosol Air Qual. Res.* 17: 406–411.
- Karlsson, H., Gustafsson, J., Cronholm, P. and Möller, L. (2009). Size-dependent toxicity of metal oxide particles – A comparison between nano- and micrometer size. *Toxicol. Lett.* 188: 112–118.
- Kim, H.T., Jung, C.H., Oh, S.N. and Lee, K.W. (2001). Particle removal efficiency of gravitational wet scrubber considering diffusion, interception, and impaction. *Environ. Eng. Sci.* 18: 125–136.
- Kittelson, D.B. (1997). Engines and nanoparticles: A review. *J. Aerosol Sci.* 29: 575–588.
- Kumar, P., Robins, A., Vardoulakis, S. and Britter, R. (2010). A review of the characteristics of nanoparticles in the urban atmosphere and the prospects for developing regulatory controls. *Atmos. Environ.* 44: 5035–5052.
- Noll, J.D., Patts, L. and Grau, R.H. (2008). The effects of ventilation controls and environmental cabs on diesel particulate matter concentrations in some limestone mines, Proc. 12th North Am. U.S. Mine Vent. Symp, 2008, pp. 463–46, <http://www.cdc.gov/niosh/mining/UseFiles/works/pdfs/teovc.pdf>.
- NTP (National Toxicology Program) (2016). Report on Carcinogens, Fourteenth Edition. Diesel Exhaust Particulates. Research Triangle Park, NC, U.S. Department of Health and Human Services, Public Health Service, <https://ntp.niehs.nih.gov/ntp/roc/content/profiles/dieselexhaustparticulates.pdf>.
- Pollock, D. and Organiscak, J. (2007). Airborne dust capture and induced airflow of various spray nozzle designs. *Aerosol Sci. Technol.* 41: 711–720.
- Pope, C.A., Thun, M.J., Namboodiri, M.M., Dockery, D.W., Evans, J.S., Speizer, F.E. and Heath, C.W. (1995). Particulate air pollution as a predictor of mortality in a prospective study of U.S. adults. *Am. J. Respir. Crit. Care Med.* 151: 669–674.
- Ran, W., Saylor, J.R. and Holt, R.G. (2013). Improved particle scavenging by a combination of ultrasonics and water sprays. *J. Aerosol Sci.* 67: 104–118.
- Ravindra, K., Sokhi, R. and Van Grieken, R. (2008). Atmospheric polycyclic aromatic hydrocarbons: Source attribution, emission factors and regulations. *Atmos. Environ.* 42: 2895–2921.
- Tetley, T.D. (2007). Health effects of nanomaterials. *Biochem. Soc. Trans.* 35: 527–531.
- Tran, H.H., Osami, N., Hirotsugu, F. and Wataru, H. (2009). Prediction for diesel particulate matter (DPM) collection efficiency of electrostatic water spraying scrubber. *J. JIME.* 44: 808–815.
- Tsai, C.J., Lin, C.H., Wang, Y.M., Hunag, C.H., Li, S.N., Wu, Z.X. and Wang, F.C. (2005). An efficient venturi scrubber system to remove submicron particles in exhaust gas. *J. Air Waste Manage. Assoc.* 55: 319–325.
- Tsai, J.H., Chen, S.J., Huang, K.L., Chaung, H.C., Lin, W.Y., Lin, C.C., Wu, T.Y., Yang, C.H. and Chiu, J.Y. (2015). Biological toxicities of exhausts from a diesel-generator fueled with water-containing acetone/butanol and waste-edible-oil-biodiesel blends. *Aerosol Air Qual. Res.* 15: 2668–2775.
- U.S. Department of Labor (2013). Diesel Exhaust/Diesel Particulate Matter; https://www.osha.gov/dts/hazardalerts/diesel_exhaust_hazard_alert.html.
- Warheit, D.B., Seidel, W.C., Carakostas, M.C. and Hartsky, M.A. (1990). Attenuation of perfluoropolymer fume pulmonary toxicity: Effect of filters, combustion method, and aerosol age. *Exp. Mol. Pathol.* 52: 309–329.

Received for review, March 1, 2017

Revised, May 15, 2017

Accepted, May 18, 2017